

# Disassembling of TEMPO-oxidized cellulose fibers: intersheet and interchain interactions in the isolation of nanofibers and unitary chains

Gustavo H. Silvestre<sup>1</sup>, Lidiane O. Pinto<sup>2</sup>, Juliana S. Bernardes<sup>2,3</sup>, Roberto H. Miwa<sup>1</sup>, and Adalberto Fazzio<sup>2,3</sup>

<sup>1</sup>*Instituto de Física, Universidade Federal de Uberlândia, C.P. 593, 38400-902, Uberlândia, MG, Brazil*

<sup>2</sup>*Brazilian Nanotechnology National Laboratory (LNNano),*

*Brazilian Center for Research in Energy and Materials (CNPem), Campinas, SP, 13083-970, Brazil and*

<sup>3</sup>*Center for Natural and Human Sciences, Federal University of ABC, Santo André, São Paulo 09210-580, Brazil*

(Dated: November 19, 2021)

Cellulose disassembly is an important issue in designing nanostructures using cellulose-based materials. In this work, we present a joint of experimental and theoretical study addressing the disassembly of cellulose nanofibrils. Through 2,2,6,6-tetramethylpiperidine-1-oxyl (TEMPO) mediated oxidation processes, combined with atomic force microscopy results, we find the formation of nanofibers with diameters corresponding to a single cellulose polymer chain. The formation of these polymer chains is ruled by repulsive electrostatic interactions between the oxidized chains. Further first-principles calculations have been done in order to provide an atomistic understanding the cellulose disassembling processes, focusing on the balance of the interchain and intersheet interactions upon oxidation. Firstly we analyse these interaction in pristine systems, where we found the intersheet interaction stronger than the interchain one. In the oxidized systems, we have considered the formation of (charged) carboxylate groups along the inner sites of elementary fibrils. We show a net charge concentration on the carboxylate groups, supporting the emergence of repulsive electrostatic interactions between the cellulose nanofibers. Indeed, our total energy results show that the weakening of the binding strength between the fibrils is proportional to the concentration and the net charge density of the carboxylate group. Moreover, by comparing interchain and intersheet binding energies, we found that most of the disassembly processes should take place by breaking the interchain O-H $\cdots$ O hydrogen bond interactions, and thus supporting the experimental observation of single and double cellulose polymeric chains.

## I. INTRODUCTION

Cellulose, the most abundant plant material resource, is a homopolymer with linear chains of glucopyranose rings linked through  $\beta$ -(1,4)-glycosidic bonds, which interact with other macromolecules as lignin and hemicellulose, within the plant cell walls<sup>1,2</sup>. The search for more eco-friendly and energy-efficient technologies has accentuated the interest of using biomass to develop fuels, chemicals, and materials<sup>3,4</sup>. Lately, nanoscale particles cellulose nanofibers (CNF) and cellulose nanocrystals (CNC) extracted from cellulose fibers by refinement have attracted attention as a next-generation material due to their outstanding mechanical properties<sup>5,6</sup>.

The resistance of plant biomass to breakdown and to fractionate into its molecular constituents is denominated recalcitrance<sup>3,7</sup>. The biopolymers assemble in the cell wall, forming a robust microstructure hardy to physical, chemical, and enzymatic processes. Partially crystalline cellulose fibers are significant contributors to recalcitrance<sup>8</sup>. Thus, an understanding, at the electronic and atomic level, of the noncovalent interactions that bind the cellulosic chains is vital in designing effective refinement processes.

The combination of synchrotron X-ray and neutron diffraction of cellulose I $\beta$ , the mostly found allomorph of cellulose in higher plants, allowed to determine the most accurate position of all atoms in the unit cell, including the hydrogens<sup>9</sup>. The crystalline structure consists of two parallel chains presenting slightly different conformations and organized into packed sheets (Fig. 1). Both H-bondings within a single layer of cellulose (interchain interactions) and stacking interactions (intersheet interactions), mainly originated from vdW forces, contribute to stabilizing the cellulose crystal structure. However, there is no consensus in the literature regarding which interaction is the key player in cellulose recalcitrance<sup>10-13</sup>.

Due to the compact and rigid structure of cellulose, size-reduction is very energy-intensive and demands harsh conditions. To extract nanofibers (CNFs), high-energy mechanical disintegration methods as refining, grinding, and homogenization are often used<sup>5</sup>. Chemical<sup>14</sup> and enzymatic treatments<sup>15</sup>, before mechanical action, are promising strategies to reduce the recalcitrance of cellulose. An established type of chemical pre-treatment consists of adding carboxylate groups (COO<sup>-</sup>) on the surface of cellulose through TEMPO-mediated oxidation<sup>14</sup>. This surface modification is particularly interesting since it displays position-selective catalytic oxidation under moderate aqueous conditions. Electrostatic repulsion and osmotic effects acting between anionically-charged surfaces lead to the formation of individualized nanofibers after the mechanical process. In a recent work<sup>16</sup>, we observed that accomplishing TEMPO-mediated oxidation under a high concentration of NaClO, cellulose nanofibers from sugarcane bagasse were obtained without a mechanical defibrillation step. Besides, a significant number of nanofibers with diameters smaller than that corresponding to an elementary fibril (< 3.5 nm) were imaged by atomic force microscopy (AFM), suggesting that besides promoting

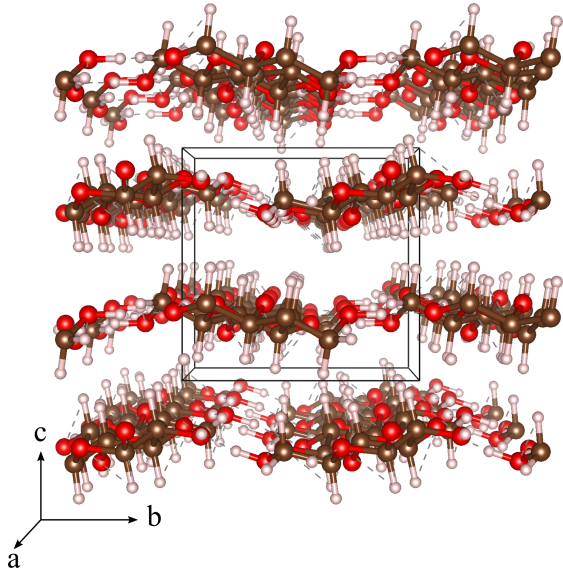


FIG. 1. Structural model of monoclinic cellulose  $I_{\beta}$ . Solid lines show a perspective view of the periodic unit cell.

the disassembling of the fiber bundles into individual elementary nanofibers, the chemical oxidation also affects the intersheet and interchain interactions.

In this work, we performed a joint of experimental and theoretical investigation of cellulose disassembly upon oxidation, and the role played by the carboxylate groups on the intersheet (IS) and interchain (IC) interactions along the inner sites of the CNFs. Firstly, through TEMPO-mediated oxidation and based on AFM measurements, we show the formation of nanofibers with widths corresponding to the ones of single and double cellulose polymer chains. In the sequence, based on first-principles calculations, we present a total energy picture of the intersheet (IS) and interchain (IC) interactions along the (i) pristine and (ii) oxidized cellulose nanofibers. In (i), we have compared the IS and IC binding energies by using different approaches to describe the long-range van der Waals (vdW) interactions, and in (ii) we have examined the strength of the IS and IC interactions as a function of the degree of oxidation of the carboxylate groups.

## II. MATERIALS AND METHODS

### A. Experimental section

#### 1. Cellulose Nanofibers Preparation

CNFs were isolated by a procedure described elsewhere<sup>16</sup>. Briefly, the cellulose pulp extracted from sugarcane bagasse was surface-carboxylated by TEMPO oxidation reaction using three volumes of a 12% (w/v) NaClO solution (16.0, 78.0 or 156.0 mL per gram of

cellulose). The average charge density was determined by three conductometric titration measurements, as previously described<sup>17</sup>. Oxidized samples from sugarcane bagasse (SC) were identified as SC-5, SC-25 and SC-50, according to the concentration of NaClO used in the reaction (5, 25 or 50 mmol/g substrate).

#### 2. Morphology characterization

The morphology of oxidized CNFs was observed by atomic force microscopy (Park NX10) under ambient conditions and using the tapping mode. The cantilever from Nanoworld had a spring constant of  $42 \text{ Nm}^{-1}$  and nominal resonance frequency of 75 kHz. Prior AFM analyses, a droplet of aqueous diluted CNF suspension ( $10 \mu\text{L}$ , 5 mg/L) was deposited onto cleaved mica substrate (TED PELLA) and dried by natural evaporation at room temperature. The length and height of CNFs were measured via Gwyddion 2.54 software by counting about 300 independent nanofibers.

### B. Computational details

The calculations were performed by using the Density Functional Theory (DFT), as implemented in the computational codes Quantum ESPRESSO (QE) software<sup>18</sup>, and Vienna *ab initio* software package (VASP)<sup>19,20</sup>. The exchange-correlation term was described within the generalized gradient approximation as proposed by Perdew, Burke and Ernzerhof (GGA-PBE)<sup>21</sup>. The periodic boundary conditions were satisfied using the super-cell approach with a vacuum region in the direction perpendicular to the cellulose sheet of at least  $12 \text{ \AA}$  to avoid image interactions. The Kohn-Sham (KS) orbitals were expanded in a plane wave basis set with an energy cutoff of 48 Ry. We have verified the convergence of our results by increasing the energy cutoff up to 60 Ry. The electron-ion interactions were solved using the Projector Augmented Wave (PAW) method<sup>22</sup>, and the 2D Brillouin Zone (BZ) is sampled according to the Monkhorst-Pack method<sup>23</sup>, using a gamma-centered  $3 \times 3 \times 1$  mesh for the cellulosic sheets and chains, and  $3 \times 3 \times 3$  for the cellulose crystalline phase. To determine the equilibrium configurations, the atomic positions and the lattice vectors were fully relaxed, considering a convergence criteria of  $25 \text{ meV \AA}^{-1}$  for the atomic forces on each atom, and pressure smaller than 0.5 Kbar.

In order to perform a thorough study of the role played by the van der Waals (vdW) forces in the structural stability of the cellulose nanofibers, we have taken into account different approaches for the vdW interactions, *viz.*: (i) vdW density functional (vdW-DF)<sup>24-27</sup> implemented in the QE and VASP codes, (ii) parameterized vdW-D2<sup>28</sup> implemented in the QE code, (iii) vdW-DF2<sup>29</sup>, and (iv) vdW-optB86b<sup>30,31</sup> both implemented in the VASP code.

### III. RESULTS AND DISCUSSIONS

#### A. Experimental results

##### 1. Overview of the cellulose nanofibers

The oxidized CNFs were isolated from sugarcane bagasse pulp through TEMPO-mediated oxidation using high oxidant content, 25 and 50 mmol/g. This reaction converts C6 primary hydroxyls groups from cellulose to carboxylates ( $\text{COO}^-$ )  $\text{Na}^+$ , yielding gravimetrically normalized values of 1.10 and 1.40 mmol of  $\text{COO}^-$  per gram of cellulose, respectively, which correspond to ca 25% of oxidation. Electrostatic repulsion between highly charged cellulose microfibrils (SC-25 and SC-50) potentials ca  $-65$  mV in water) together with osmotic effects promoted the disassembling of completely individualized CNF dispersed in water without the need for high-energy mechanical treatments, as can be visualized in Fig.2(a). On the other hand, cellulose fibers with low carboxylate content (SC-5, 0.4 mmol per gram of cellulose) presented aggregated fibril bundles, as already observed for different types of biomass. The SC-25 and SC-50 nanofibers present average lengths in the range of 243-370 nm and an average width of 4 nm, which may correspond to elementary fibrils diameter, according to Ding and Himmel's model for maize biomass<sup>32</sup>.

Further, height histograms of AFM images show a significant number of nanoelements with widths of less than the elementary fibril diameter [Fig. 2(b)]. This result suggests that in addition to disassembling the bundles, the oxidation may also weaken the noncovalent interchain and intersheet interactions within the elementary fibril, leading to the release of nanofibers with widths that correspond about to single (0.44 nm) and double (0.88 nm) cellulose polymer chains<sup>33</sup>, as indicated by the arrows in Fig.2(c). The width distribution may be an outcome of non-uniform distribution of charges along the fibers, as pointed out by Paajevan *et al.*<sup>34</sup>. In addition to promoting the detachment of polymer chains, harsh oxidation reactions (SC-25 and SC-50) reduce the mass recovery ratio of TEMPO-oxidized pulps to ca 40 % compared to milder conditions (SC-5). This reduction is probably due to the removal of water-soluble molecules produced during oxidation, as discussed in our previous study<sup>16</sup>. Water-soluble products from TEMPO-oxidized cellulose pulps were also extracted by Hirota *et al.* using surface peeling with a solution of 20 % aqueous NaOH<sup>35</sup>.

#### B. Theoretical modeling

The present experimental results suggest that the formation of cellulose polymer chains is a consequence of the weakening of (noncovalent) intersheet and interchain interactions within the elementary oxidized fibrils. Thus, in order to provide further support to these findings,

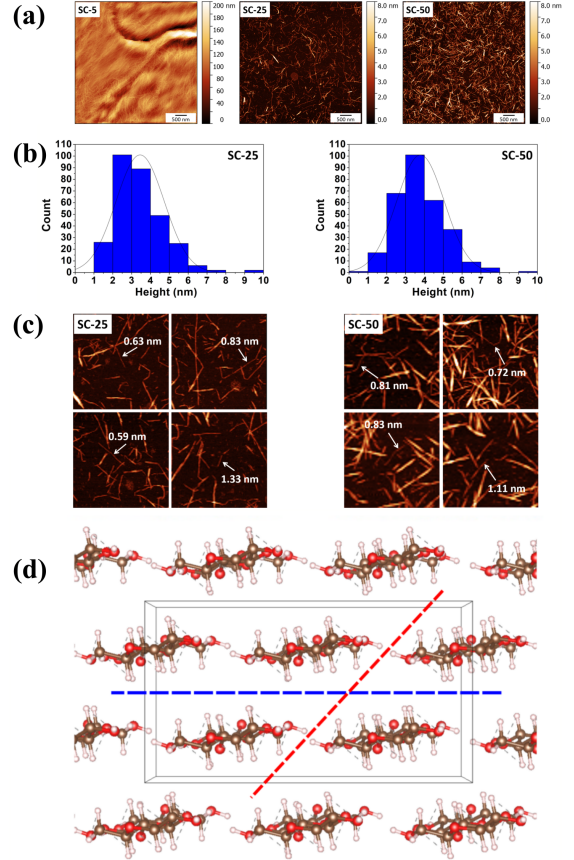


FIG. 2. Experimental results: AFM images (a) and (c), and elementary fibril diameter distribution (b). Representation of an inner sites of cellulose crystal (d). The red (black) dashed lines indicates a interchain (intersheet) disruption.

we have performed first-principles DFT simulations, as described in Sec.II-B, addressing these noncovalent interactions. Firstly, we start our investigation with the pristine system, focusing on the role played by the hydrogen bonds and vdW forces in the strength of intersheet/interchain interactions. In the sequence, we examine the changes of these IS and IC interactions upon the presence of charged carboxylate groups embedded within elementary fibrils. We present an atomistic picture of how these charged carboxylate groups rule the repulsive electrostatic forces within the nanofibrils, which in its turn weakens the noncovalent (IS and IC) interactions between the polymeric cellulose chains.

##### 1. Pristine cellulose nanofibers

In Fig.1 we present the structural model of the monoclinic  $I_\beta$  phase, where the periodic structure can be described by two misaligned molecular chains per unit-cell. The cellulosic sheets are composed of linear chains parallel to the **a** direction, where the lateral interchain interaction (**b** direction) are mostly ruled by  $\text{O}-\text{H}\cdots\text{O}$  hy-

TABLE I. Intersheet (IS), interchain (IC), and CNF binding energies for pristine CNFs, using vdW-DF, -D2 approaches implemented in the QE code, and without vdW. The binding energies are in eV/unit-chain.

vdW	$E_{\text{IS}}^b$	$E_{\text{IC}}^b$	$E_{\text{CNF}}^b$	$E_{\text{IS}}^b/E_{\text{IC}}^b$
DF	-1.351	-0.676	-2.027	2.0
D2	-1.080	-0.833	-1.913	1.3
no vdW	-0.127	-0.569	-0.697	0.2

TABLE II. Equilibrium geometry of  $I_\beta$  cellulose.

vdW	DF	D2	Exp. <sup>9</sup>
$a$ (Å)	7.872	7.413	7.784
$b$ (Å)	8.391	8.159	8.201
$c$ (Å)	10.576	10.416	10.380
$\alpha$ (°)	90.0	89.8	–
$\beta$ (°)	89.8	89.9	–
$\gamma$ (°)	93.5	95.5	96.5

drogen bonds (HBs); while vdW interaction brings the main contribution to the structural stability to the sheet staking along the normal direction (**c**). The strength of the intersheet (IS) and interchain (IC) interactions were quantified by the calculation of the IS and IC binding energies ( $E_{\text{IS}}^b$  and  $E_{\text{IC}}^b$ , respectively),

$$\begin{aligned} E_{\text{IS}}^b &= E_{\text{bulk}} - E_{\text{sheet}} \\ E_{\text{IC}}^b &= E_{\text{sheet}} - E_{\text{chain}}. \end{aligned}$$

$E_{\text{bulk}}$ ,  $E_{\text{sheet}}$ , and  $E_{\text{chain}}$  are the total energies of crystalline cellulose nanofibers, free-standing cellulosic sheet, and free-standing single molecular chain. The binding energy of the cellulose nanofibers ( $E_{\text{CNF}}^b$ ) can be written as:  $E_{\text{CNF}}^b = E_{\text{IC}}^b + E_{\text{IS}}^b$ . By using the vdW-DF approach<sup>24–27</sup>, we found  $E_{\text{CNF}}^b = -2.027$  eV/unit-chain (unit-chain corresponds to two glucose rings)<sup>36</sup>. Our total energy results are summarized in Table I, where we have also considered the semi-empirical vdW-D2<sup>28</sup> approach, to describe the long-range dispersive interactions. In Table II, we present key informations regarding the equilibrium geometry of the  $I_\beta$  crystalline cellulose, where we find a good agreement with the experimental measurements performed by Nishiyama *et al.*<sup>9</sup>.

Focusing on the IS and IC binding energies, there is a lack of consensus regarding the energetic balance between IS and IC interactions, where we may find different results obtained through different calculation approaches. For instance, Qian *et al.*<sup>10</sup> found IC interaction stronger than the IS interaction; while Parthasarathi *et al.*<sup>37</sup> obtained nearly the same contribution for both interactions. Meanwhile, even upon the inclusion of vdW correction<sup>28</sup>, Li *et al.*<sup>12</sup> obtained 0.8 and 1.1 eV/unit-chain, for IS and IC interactions, respectively. In contrast, based on molecular dynamic (MD) simulations, Gross and Chu<sup>11,38</sup> pointed out that the IS interaction is larger than IC interaction. Our total energy results

support these latter findings. We found that the IS interaction is stronger than the IC one by almost twice,  $E_{\text{IS}}^b/E_{\text{IC}}^b \approx 2$  (vdW-DF results). By using the vdW-D2 approach, the strength of the IS (IC) interaction reduces (increases), however keeping  $E_{\text{IS}}^b$  larger than  $E_{\text{IC}}^b$  with  $E_{\text{IS}}^b/E_{\text{IC}}^b \approx 1.3$ . To check the accuracy of our results, we have calculated the binding energies using other non-local self-consistent vdW approaches. These results are summarized in Table III.

As pointed out by Gross and Chu, vdW interaction rules the IS interaction, while it presents a minor contribution to the IC one. In order to provide a quantitative picture of the role played by the dispersive forces to the structural stability of the  $I_\beta$  CNFs, we calculate  $E_{\text{IS}}^b$  and  $E_{\text{IC}}^b$  by turning-off the vdW contribution, but keeping the equilibrium geometry obtained by the vdW-DF calculation. Here, we found that the strength of the IS interaction reduces from  $-1.351$  to  $-0.127$  eV/unit-chain, while for the IC interactions change by less than 0.1 eV,  $E_{\text{IC}}^b = -0.676 \rightarrow -0.569$  eV/unit-chain. Thus, revealing that vdW forces present (i) a dominant role on the energetic stability between the cellulosic sheets (about 90% of the IS interactions), and (ii) a minor contribution to the IC interactions ( $\sim 16\%$ ). These findings [(i) and (ii)] will be helpful to provide an energetic picture for the disintegration of oxidized CNFs as discussed below.

We are aware that the presence of solvents may contribute to the energetic stability involving cellulose interfaces. For instance, the role played by water molecules on the energetic stability of cellulose/lipid interfaces<sup>39,40</sup>, and the reorganization processes of cellulose sheets<sup>41,42</sup>. In the present study we have not included the contribution of solvent in the calculations of the binding energies. Here,  $E_{\text{IC}}^b$  and  $E_{\text{IS}}^b$  were obtained comparing the total energies, at  $T=0$ , of the initial (chain/sheet) and final (sheet/bulk) ground state configurations. We are assuming the approximation that (i) the solvent contribution to the total energies of the initial and final systems are nearly the same, as well as (ii) the temperature dependence carried out by the entropic term in the free energy. Therefore, within such an approximation, these contributions [(i) and (ii) separately] are canceled out when we compare the initial and final free energies<sup>43,44</sup>.

## 2. Oxidized cellulose nanofibers

The energy cost to disintegrate the cellulose fibers reduces upon the formation of charged carboxylate groups ( $\text{COO}^-$ )<sup>45</sup>. Indeed, previous experimental works have shown the disintegration of cellulose into nanofibers with diameters of 3–5 nm mediated by (TEMPO) oxidation processes<sup>46,47</sup>. In parallel, MD simulations have been done addressing the effect of the presence of carboxylate groups, bonded to the CNF surfaces, on the inter-fibril interaction<sup>34</sup>. Here, we have used a recently proposed low energy cost pathway<sup>16</sup> to produce cellulose nanofibers with widths of single and double cellulose polymer chains,

TABLE III. Intersheet (IS), and interchain (IC), and CNF binding energies using the vdW-DF, -DF2, and -optB86b approaches implemented in the VASP code. The binding energies are in eV/unit-chain.

vdW	$E_{IS}^b$	$E_{IC}^b$	$E_{CNF}^b$	$E_{IS}^b/E_{IC}^b$
DF	-1.288	-0.663	-1.951	1.9
DF2	-1.232	-0.716	-1.948	1.7
optB86b	-1.441	-0.818	-2.259	1.8

as depicted in Fig. 2.

Given such a scenario, and the present experimental findings, it is expected that the formation of carboxylate groups should take place not only on the surface of the elementary fibrils, but also at the inner sites of the CNFs [indicated by dashed lines in Fig. 2(d)], weakening the intersheet and interchain interactions.

The calculation procedure of the IS and IC binding energy, as a function of the charging state of the carboxylate group, is schematically shown in Figs. 3(a) and (b). Here, the binding energy ( $E^b$ ) corresponding to the IS [IC] interaction was obtained by comparing the total energies of two free-standing cellulosic sheets [chains] interacting to each other (final configuration), as shown in Fig. 3(a1) [3(b1)], and the ones far from each other (initial configuration), Fig. 3(a2) [3(b2)], for a given charging state ( $q$ )<sup>48</sup>,

$$E_{IS/IC}^b(q) = E_{\text{final}}(q) - E_{\text{initial}}(q).$$

For each configuration (initial/final), the fully relaxed atomic positions, and the total energies were obtained including the vdW interactions within the vdW-DF approach<sup>24-27</sup>. Within our supercell approach, we have considered the presence of carboxylate groups with different concentrations ( $[\text{COO}^-]$ ), as shown in Figs. 3(c1)-(c4). The localization of the net charge ( $q$ ) was determined by using the Löwdin orbital population<sup>49</sup>, where we found that most of charging lies on the carboxylate groups. In Figs. 4(a) and (b), we present the increase of the net charge density along a cellulose chain with  $[\text{COO}^-]$  of 50% when the charging state increases from  $q=0.25 \rightarrow 0.50 e$  and  $q=0.50 \rightarrow 1.00 e$ . To check the adequacy of our calculation approach, instead of charging our supercell, we have considered the presence of sodium ions nearby the carboxylate groups<sup>34</sup>. In this case, we found a net charging of about  $0.5 e$  per  $[\text{COO}^-]$  unit. Here, we have not considered the disordered structures present at the edge sites of the CNFs. Eventually, the formation of carboxylate groups at the edge sites may trigger the disassembling process. However, the role played by the oxidized sites, weakening the IC and IS interaction, should be the same as those we have predicted for the inner sites of the CNFs.

Our results of binding energies for the IS and IC interactions [Figs. 5(a) and (b)] reveal that the weakening of the IS and IC interactions, compared with the ones of pristine systems (dashed lines in Fig. 5), is propor-

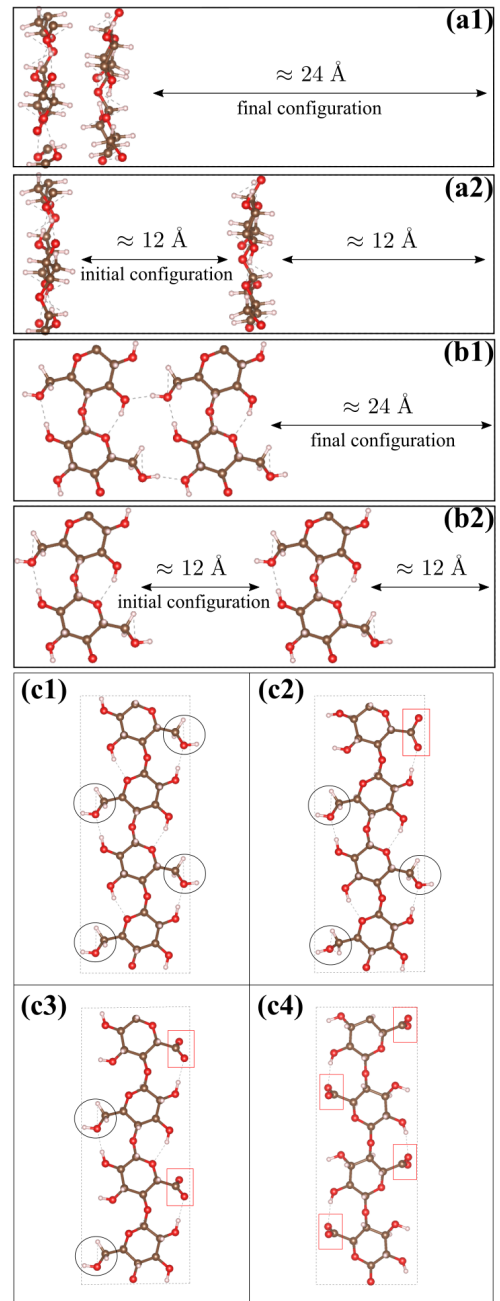


FIG. 3. Schematic representation of the IS (a) and IC (b) binding energy calculations. (a1)-(b1)/(a2)-(b2) Final/Initial configuration of two free standing cellulosic sheets (a) and chains (b). (c) Structural models of pristine (non-oxidized) NC chain (c1), and oxidized chains with linear concentration of carboxylate groups of  $[\text{COO}^-] = 25\%$  (c2),  $50\%$  (c3), and  $100\%$  (c4). The carboxylate groups are within rectangles.

tional to the charging and the concentration of carboxylate groups, which is in line with our experimental findings. As shown in Section III-A, the formation of cellulose polymer chains takes place in SC-25 and -50, but not in SC-5 due to its low concentration of charged carboxylated sites. Moreover, the net (negative) charge localiza-

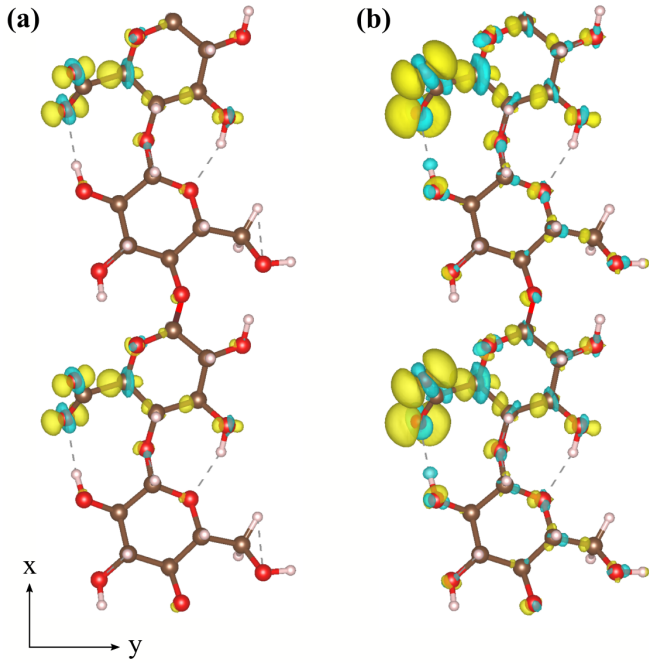


FIG. 4. Charge density distribution along oxidized cellulose chain, with  $[\text{COO}^-]$  of 50%, upon the net charging increase  $q=0.25 \rightarrow 0.50 e$  (a) and  $q=0.25 \rightarrow 1.0 e$  (b). Isosurfaces of  $0.003 e/\text{\AA}^3$  in (a) and  $0.002 e/\text{\AA}^3$  in (b).

tion in the carboxylate group, as shown in Fig. 4, indeed, support the repulsive electrostatic role on the cellulose disassembling process of CNF by weakening the IS and IC interactions<sup>45</sup>.

Further binding energy comparison [Fig. 5(c)] shows that, in general, the IC interactions are more sensitive to the oxidation than the IS interactions. For instance, for  $[\text{COO}^-]=50\%$  and charging of  $q = 0.5e$  the IC binding energy reduces by  $0.25 \text{ eV/unit-chain}$ ,  $E_{\text{IC}}^b = -0.48 \rightarrow -0.23 \text{ eV/unit-chain}$ , whereas for the IS interaction we found  $E_{\text{IS}}^b$  reduces by  $0.09 \text{ eV/unit-chain}$ ,  $-0.60 \rightarrow -0.51 \text{ eV/unit-chain}$ . These results not only support the present experimental findings (summarized in Fig. 2) but also allow us to infer that the CNF disassembly should take place (preferentially) through a disruption of the interchain interactions [indicated by red dashed lines in Fig. 2(d)].

As we have discussed above, in the pristine systems, the IS binding energy is mostly dictated by vdW forces, while the hydrogen-like  $\text{C-H}\cdots\text{O}$  bonds bring a minor contribution. In contrast, the IC binding strength is mostly ruled by  $\text{O-H}\cdots\text{O}$  hydrogen bonds, followed by a minor contribution from vdW forces. Since, in the oxidized systems,  $E_{\text{IC}}^b$  presents greater reduction compared with  $E_{\text{IS}}^b$  [Fig. 5(c)], here we can infer that the weakening  $\text{O-H}\cdots\text{O}$  and  $\text{C-H}\cdots\text{O}$  bonds play the main role in the disassembly process of CNFs. In order to provide a qualitative support to such a statement, we calculate  $E_{\text{IS/IC}}^b(q)$ , for  $[\text{COO}^-]=50\%$ , with no vdW contribution to the total energies. Our results for the IS

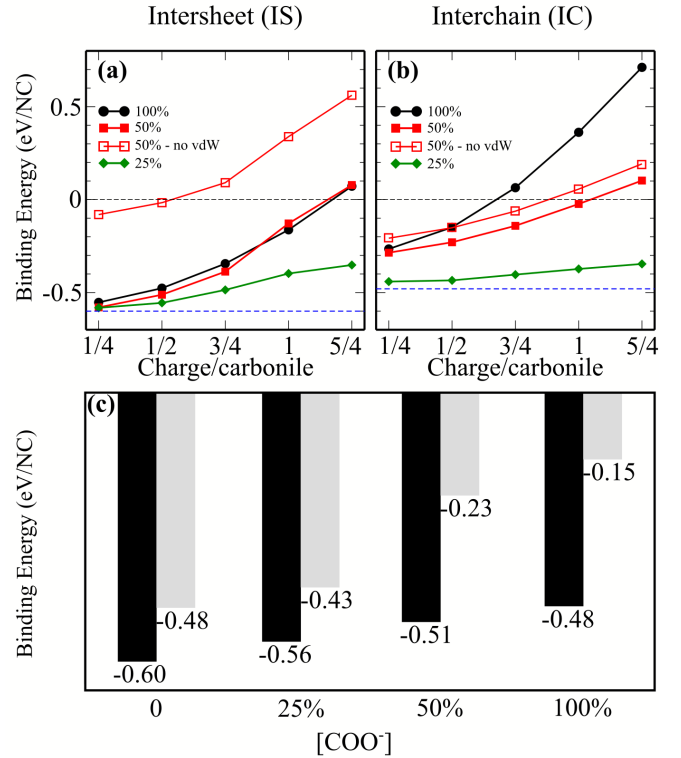


FIG. 5. Intersheet (a) and interchain (b) binding energy as a function of the charging state ( $q$ ) with  $[\text{COO}^-]=100, 50$ , and  $25\%$ . Dashed lines indicate the calculated binding energies of a (non-oxidized) pristine system. (c) IS (black) and IC (shaded) binding energies for  $q = 0.5e$ .  $[\text{COO}^-] = 0$  indicates non-oxidized pristine system.

and IC binding energies [indicated by empty squares in Figs. 5(a) and (b)] reveal a significant reduction of the former. For instance, for  $q = 0.5e$ ,  $E_{\text{IS}}^b(q)$  reduces from  $-0.511$  to  $-0.016 \text{ eV/unit-chain}$ , whereas the strength of the IC interaction reduces by about  $0.08 \text{ eV/unit-chain}$ ,  $E_{\text{IC}}^b(q) = -0.230 \rightarrow -0.151 \text{ eV/unit-chain}$ . In other words, the higher reduction of  $E_{\text{IS}}^b$  compared with that of  $E_{\text{IC}}^b$  is a consequence of the predominance of van der Waals forces in the intersheet interactions.

We have used the current state-of-the-art DFT-vdW approach to describe the non-covalent interactions<sup>50,51</sup>, however, there are other “ingredients” that we have not considered in the present study of oxidized CNFs. (i) Water molecules; the preferential incorporation of water molecules at the hydrophilic regions, of the CNFs, may favor the formation of cellulose chains instead of sheets<sup>52</sup>. (ii) Hydrated (positively charged) counter-ions, like  $[\text{Na}(\text{H}_2\text{O})_n]^+$ <sup>34,44,53-55</sup>, resulting in a screening effect of the repulsive electrostatic interaction between the negatively charged carboxylate groups. Further investigations are necessary including (i) and (ii), combined with an accurate description of the noncovalent vdW interactions, in order to provide a more complete picture of the formation of cellulose polymer chains. However, despite the lack of these “ingredients”, we believe that our

simulations results are valuable for providing not only theoretical support to the experimental findings, but also an atomic scale understanding of the disassembling processes in oxidized CNFs.

#### IV. SUMMARY AND CONCLUSIONS

We have performed an experimental and theoretical combined investigation of cellulose disassembly mediated oxidation processes. Based on a low energy cost pathway, single and double cellulose polymers chains have been synthesized from oxidized cellulose nano fibers (CNFs). Such a disruption of CNFs was attributed to the formation of carboxylate groups embedded within oxidized fibrils, weakening the noncovalent interchain (IC) and intersheet (IS) interactions. We have shown that the disassembling process depends on the concentration of the carboxylate groups. First-principles DFT calculations revealed that, indeed, the IC and IS binding energies  $[E_{IC/IS}^b(q)]$  reduce in the oxidized CNFs. We find

that such a reduction of  $E_{IC/IS}^b(q)$  is proportional to the charging state ( $q$ ), and the concentration of the oxidized carboxylate groups indicating an electrostatic repulsion between the (charged) cellulose fibrils. Finally, comparing the IS and IC binding energies, we found that the disassembly processes of the oxidized CNFs should take place mostly through a disruption of the interchain interactions, giving rise to (predominantly) fibers and cellulose chains, instead of sheets, as a final structure, and thus in accordance/supporting with the present experimental AFM observations.

#### ACKNOWLEDGMENTS

The authors acknowledge financial support from the Brazilian agencies CNPq, FAPEMIG, and FAPESP (grant 16/04514-7 and 17/02317-2), and the LNCC (SCAFMat2), CENAPAD-SP for computer time.

- 
- [1] N. G. Taylor, "Cellulose biosynthesis and deposition in higher plants," *New Phytologist*, vol. 178, no. 2, pp. 239–252, 2008.
- [2] E. J. Mellerowicz and T. A. Gorshkova, "Tensional stress generation in gelatinous fibres: a review and possible mechanism based on cell-wall structure and composition," *Journal of experimental botany*, vol. 63, no. 2, pp. 551–565, 2012.
- [3] M. E. Himmel, S.-Y. Ding, D. K. Johnson, W. S. Adney, M. R. Nimlos, J. W. Brady, and T. D. Foust, "Biomass recalcitrance: engineering plants and enzymes for biofuels production," *science*, vol. 315, no. 5813, pp. 804–807, 2007.
- [4] H. Jørgensen, J. B. Kristensen, and C. Felby, "Enzymatic conversion of lignocellulose into fermentable sugars: challenges and opportunities," *Biofuels, Bioproducts and Biorefining*, vol. 1, no. 2, pp. 119–134, 2007.
- [5] D. Klemm, F. Kramer, S. Moritz, T. Lindström, M. Ankerfors, D. Gray, and A. Dorris, "Nanocelluloses: a new family of nature-based materials," *Angewandte Chemie International Edition*, vol. 50, no. 24, pp. 5438–5466, 2011.
- [6] Y. Habibi, L. A. Lucia, and O. J. Rojas, "Cellulose nanocrystals: chemistry, self-assembly, and applications," *Chemical reviews*, vol. 110, no. 6, pp. 3479–3500, 2010.
- [7] X. Zhao, L. Zhang, and D. Liu, "Biomass recalcitrance. part i: the chemical compositions and physical structures affecting the enzymatic hydrolysis of lignocellulose," *Biofuels, Bioproducts and Biorefining*, vol. 6, no. 4, pp. 465–482, 2012.
- [8] A. Zoghalmi and G. Paës, "Lignocellulosic biomass: understanding recalcitrance and predicting hydrolysis," *Frontiers in Chemistry*, vol. 7, p. 874, 2019.
- [9] Y. Nishiyama, P. Langan, and H. Chanzy, "Crystal structure and hydrogen-bonding system in cellulose  $i\beta$  from synchrotron x-ray and neutron fiber diffraction," *Journal of the American Chemical Society*, vol. 124, no. 31, pp. 9074–9082, 2002.
- [10] X. Qian, S.-Y. Ding, M. R. Nimlos, D. K. Johnson, and M. E. Himmel, "Atomic and electronic structures of molecular crystalline cellulose  $i\beta$ : A first-principles investigation," *Macromolecules*, vol. 38, no. 25, pp. 10580–10589, 2005.
- [11] A. S. Gross and J.-W. Chu, "On the molecular origins of biomass recalcitrance: the interaction network and solvation structures of cellulose microfibrils," *The Journal of Physical Chemistry B*, vol. 114, no. 42, pp. 13333–13341, 2010.
- [12] Y. Li, M. Lin, and J. W. Davenport, "Ab initio studies of cellulose i: crystal structure, intermolecular forces, and interactions with water," *The Journal of Physical Chemistry C*, vol. 115, no. 23, pp. 11533–11539, 2011.
- [13] A. Devarajan, S. Markutsya, M. H. Lamm, X. Cheng, J. C. Smith, J. Y. Baluyut, Y. Kholod, M. S. Gordon, and T. L. Windus, "Ab initio study of molecular interactions in cellulose  $i\alpha$ ," *The Journal of Physical Chemistry B*, vol. 117, no. 36, pp. 10430–10443, 2013.
- [14] T. Saito, S. Kimura, Y. Nishiyama, and A. Isogai, "Cellulose nanofibers prepared by tempo-mediated oxidation of native cellulose," *Biomacromolecules*, vol. 8, no. 8, pp. 2485–2491, 2007.
- [15] M. Pääkkö, M. Ankerfors, H. Kosonen, A. Nykänen, S. Ahola, M. Österberg, J. Ruokolainen, J. Laine, P. T. Larsson, O. Ikkala, *et al.*, "Enzymatic hydrolysis combined with mechanical shearing and high-pressure homogenization for nanoscale cellulose fibrils and strong gels," *Biomacromolecules*, vol. 8, no. 6, pp. 1934–1941, 2007.
- [16] L. O. Pinto, J. S. Bernardes, and C. A. Rezende, "Low-energy preparation of cellulose nanofibers from sugarcane bagasse by modulating the surface charge density," *Car-*

- bohydrate polymers*, vol. 218, pp. 145–153, 2019.
- [17] N. Lin, C. Bruzzese, and A. Dufresne, “Tempo-oxidized nanocellulose participating as crosslinking aid for alginate-based sponges,” *ACS applied materials & interfaces*, vol. 4, no. 9, pp. 4948–4959, 2012.
- [18] P. Giannozzi, S. Baroni, N. Bonini, M. Calandra, R. Car, C. Cavazzoni, D. Ceresoli, G. L. Chiarotti, M. Cococcioni, I. Dabo, *et al.*, “Quantum espresso: a modular and open-source software project for quantum simulations of materials,” *Journal of physics: Condensed matter*, vol. 21, no. 39, p. 395502, 2009.
- [19] G. Kresse and J. Furthmüller, “Efficiency of ab-initio total energy calculations for metals and semiconductors using a plane-wave basis set,” *Computational materials science*, vol. 6, no. 1, pp. 15–50, 1996.
- [20] G. Kresse and J. Furthmüller, “Efficient iterative schemes for ab initio total-energy calculations using a plane-wave basis set,” *Physical review B*, vol. 54, no. 16, p. 11169, 1996.
- [21] J. P. Perdew, K. Burke, and M. Ernzerhof, “Generalized gradient approximation made simple,” *Physical review letters*, vol. 77, no. 18, p. 3865, 1996.
- [22] P. E. Blöchl, “Projector augmented-wave method,” *Physical review B*, vol. 50, no. 24, p. 17953, 1994.
- [23] H. J. Monkhorst and J. D. Pack, “Special points for brillouin-zone integrations,” *Physical review B*, vol. 13, no. 12, p. 5188, 1976.
- [24] T. Thonhauser, S. Zuluaga, C. Arter, K. Berland, E. Schröder, and P. Hyldgaard, “Spin signature of non-local correlation binding in metal-organic frameworks,” *Physical review letters*, vol. 115, no. 13, p. 136402, 2015.
- [25] T. Thonhauser, V. R. Cooper, S. Li, A. Puzder, P. Hyldgaard, and D. C. Langreth, “Van der waals density functional: Self-consistent potential and the nature of the van der waals bond,” *Physical Review B*, vol. 76, no. 12, p. 125112, 2007.
- [26] K. Berland, V. R. Cooper, K. Lee, E. Schröder, T. Thonhauser, P. Hyldgaard, and B. I. Lundqvist, “van der waals forces in density functional theory: a review of the vdW-df method,” *Reports on Progress in Physics*, vol. 78, no. 6, p. 066501, 2015.
- [27] D. Langreth, B. I. Lundqvist, S. D. Chakarova-Käck, V. Cooper, M. Dion, P. Hyldgaard, A. Kelkkanen, J. Kleis, L. Kong, S. Li, *et al.*, “A density functional for sparse matter,” *Journal of Physics: Condensed Matter*, vol. 21, no. 8, p. 084203, 2009.
- [28] S. Grimme, “Semiempirical gga-type density functional constructed with a long-range dispersion correction,” *Journal of computational chemistry*, vol. 27, no. 15, pp. 1787–1799, 2006.
- [29] I. Hamada, “van der waals density functional made accurate,” *Physical Review B*, vol. 89, no. 12, p. 121103, 2014.
- [30] J. Klimeš, D. R. Bowler, and A. Michaelides, “Chemical accuracy for the van der waals density functional,” *Journal of Physics: Condensed Matter*, vol. 22, no. 2, p. 022201, 2009.
- [31] J. Klimeš, D. R. Bowler, and A. Michaelides, “Van der waals density functionals applied to solids,” *Physical Review B*, vol. 83, no. 19, p. 195131, 2011.
- [32] S.-Y. Ding and M. E. Himmel, “The maize primary cell wall microfibril: a new model derived from direct visualization,” *Journal of agricultural and food chemistry*, vol. 54, no. 3, pp. 597–606, 2006.
- [33] I. Usov, G. Nyström, J. Adamcik, S. Handschin, C. Schütz, A. Fall, L. Bergström, and R. Mezzenga, “Understanding nanocellulose chirality and structure-properties relationship at the single fibril level,” *Nature communications*, vol. 6, no. 1, pp. 1–11, 2015.
- [34] A. Paaajanen, Y. Sonavane, D. Ignasiak, J. A. Ketoja, T. Maloney, and S. Paavilainen, “Atomistic molecular dynamics simulations on the interaction of tempo-oxidized cellulose nanofibrils in water,” *Cellulose*, vol. 23, no. 6, pp. 3449–3462, 2016.
- [35] M. Hirota, K. Furihata, T. Saito, T. Kawada, and A. Isogai, “Glucose/glucuronic acid alternating copolysaccharides prepared from tempo-oxidized native celluloses by surface peeling,” *Angewandte Chemie International Edition*, vol. 49, no. 42, pp. 7670–7672, 2010.
- [36] Increasing the energy cutoff to 60 Ry we obtained  $E_{IS}^b = -1.321$  eV/unit-chain and  $E_{IC}^b = -0.665$  eV/unit-chain, resulting in a binding energy of  $-1.986$  eV/unit-chain.
- [37] R. Parthasarathi, G. Bellesia, S. Chundawat, B. Dale, P. Langan, and S. Gnanakaran, “Insights into hydrogen bonding and stacking interactions in cellulose,” *The Journal of Physical Chemistry A*, vol. 115, no. 49, pp. 14191–14202, 2011.
- [38] A. S. Gross, A. T. Bell, and J.-W. Chu, “Thermodynamics of cellulose solvation in water and the ionic liquid 1-butyl-3-methylimidazolium chloride,” *The Journal of Physical Chemistry B*, vol. 115, no. 46, pp. 13433–13440, 2011.
- [39] A. A. Gurtovenko, E. I. Mukhamadiarov, A. Y. Kostritskii, and M. Karttunen, “Phospholipid-cellulose interactions: Insight from atomistic computer simulations for understanding the impact of cellulose-based materials on plasma membranes,” *The Journal of Physical Chemistry B*, vol. 122, no. 43, pp. 9973–9981, 2018.
- [40] A. A. Gurtovenko and M. Karttunen, “Controlled on-off switching of tight-binding hydrogen bonds between model cell membranes and acetylated cellulose surfaces,” *Langmuir*, vol. 35, no. 42, pp. 13753–13760, 2019.
- [41] H. Miyamoto, M. Umemura, T. Aoyagi, C. Yamane, K. Ueda, and K. Takahashi, “Structural reorganization of molecular sheets derived from cellulose ii by molecular dynamics simulations,” *Carbohydrate research*, vol. 344, no. 9, pp. 1085–1094, 2009.
- [42] H. Miyamoto, C. Yamane, and K. Ueda, “Structural changes in the molecular sheets along (hk0) planes derived from cellulose i  $\beta$  by molecular dynamics simulations,” *Cellulose*, vol. 20, no. 3, pp. 1089–1098, 2013.
- [43] G.-X. Qian, R. M. Martin, and D. Chadi, “First-principles study of the atomic reconstructions and energies of ga-and as-stabilized gaas (100) surfaces,” *Physical Review B*, vol. 38, no. 11, p. 7649, 1988.
- [44] M. Deshpande, R. H. Scheicher, R. Ahuja, and R. Pandey, “Binding strength of sodium ions in cellulose for different water contents,” *The Journal of Physical Chemistry B*, vol. 112, no. 30, pp. 8985–8989, 2008.
- [45] A. Tejado, M. N. Alam, M. Antal, H. Yang, and T. G. van de Ven, “Energy requirements for the disintegration of cellulose fibers into cellulose nanofibers,” *Cellulose*, vol. 19, no. 3, pp. 831–842, 2012.
- [46] T. Saito and A. Isogai, “Tempo-mediated oxidation of native cellulose. the effect of oxidation conditions on chemical and crystal structures of the water-insoluble fractions,” *Biomacromolecules*, vol. 5, no. 5, pp. 1983–1989, 2004.

- [47] T. Saito, Y. Nishiyama, J.-L. Putaux, M. Vignon, and A. Isogai, "Homogeneous suspensions of individualized microfibrils from tempo-catalyzed oxidation of native cellulose," *Biomacromolecules*, vol. 7, no. 6, pp. 1687–1691, 2006.
- [48] We check the convergence of our results with respect to the size of the supercell, since in the charged systems a jellium background of opposite charge has been inserted in order to work with neutral supercells. Here, we found that by increasing the vacuum region from 24 to 40 Å our results of  $E^b(q)$  change by  $\sim 4\%$ .
- [49] P.-O. Löwdin, "Quantum theory of many-particle systems. ii. study of the ordinary hartree-fock approximation," *Physical Review*, vol. 97, no. 6, p. 1490, 1955.
- [50] M. Stöhr, T. Van Voorhis, and A. Tkatchenko, "Theory and practice of modeling van der waals interactions in electronic-structure calculations," *Chemical Society Reviews*, vol. 48, no. 15, pp. 4118–4154, 2019.
- [51] M. Kim, T. Gould, D. Rocca, and S. Lebègue, "Establishing the accuracy of density functional approaches for the description of noncovalent interactions in biomolecules," *Physical Chemistry Chemical Physics*, vol. 22, no. 38, pp. 21685–21695, 2020.
- [52] Y. Zhang, T. Zhang, S. Kuga, M. Wu, and Y. Huang, "Polarities-induced weakening of molecular interaction and formation of nanocellulose with different dimensions," *ACS Sustainable Chemistry & Engineering*, vol. 8, no. 25, pp. 9277–9290, 2020.
- [53] J. Heyda and J. Dzubiella, "Ion-specific counterion condensation on charged peptides: Poisson–boltzmann vs. atomistic simulations," *Soft Matter*, vol. 8, no. 36, pp. 9338–9344, 2012.
- [54] J. Peng, D. Cao, Z. He, J. Guo, P. Hapala, R. Ma, B. Cheng, J. Chen, W. J. Xie, X.-Z. Li, *et al.*, "The effect of hydration number on the interfacial transport of sodium ions," *Nature*, vol. 557, no. 7707, pp. 701–705, 2018.
- [55] T. Qi, Z. Huang, H. Xie, H.-M. Yang, Z.-B. Si, Y.-J. Lyu, L.-J. Liu, J.-F. Zhang, H.-Q. Yang, and C.-W. Hu, "Co-operative interaction of sodium and chlorine ions with  $\beta$ -cellobiose in aqueous solution from quantum mechanics and molecular dynamics," *Cellulose*, vol. 27, pp. 6793–6809, 2020.